
Multivariate Conformal Prediction using Optimal Transport

Michal Klein¹ Louis Bethune¹ Eugene Ndiaye¹ Marco Cuturi¹

Abstract

Conformal prediction (CP) quantifies the uncertainty of machine learning models by constructing sets of plausible outputs. These sets are constructed by leveraging a so-called conformity score, a quantity computed using the input point of interest, a prediction model, and past observations. CP sets are then obtained by evaluating the conformity score of all possible outputs, and selecting them according to the rank of their scores. Due to this ranking step, most CP approaches rely on a score functions that are univariate. The challenge in extending these scores to multivariate spaces lies in the fact that no canonical order for vectors exists. To address this, we leverage a natural extension of multivariate score ranking based on optimal transport (OT). Our method, **OT-CP**, offers a principled framework for constructing conformal prediction sets in multidimensional settings, preserving distribution-free coverage guarantees with finite data samples. We demonstrate tangible gains in a benchmark dataset of multivariate regression problems and address computational & statistical trade-offs that arise when estimating conformity scores through OT maps.

1. Introduction

Conformal prediction (CP) (Gammerman et al., 1998; Vovk et al., 2005; Shafer & Vovk, 2008) has emerged as a simple framework to quantify the prediction uncertainty of machine learning algorithms without relying on distributional assumptions on the data. For a sequence of observed data, and a new input point,

$$D_n = \{(x_1, y_1), \dots, (x_n, y_n)\} \text{ and } x_{n+1},$$

the objective is to construct a set that contains the unobserved response y_{n+1} with a specified confidence level $100(1 - \alpha)\%$. This involves evaluating scores $S(x, y, \hat{y}) \in$

\mathbb{R} such as the prediction error of a model \hat{y} , for each observation (x, y) in D_n and ranking these score values. The conformal prediction set for the new input x_{n+1} is the collection of all possible responses y whose score $S(x_{n+1}, y, \hat{y})$ ranks small enough to meet the prescribed confidence threshold, compared to the scores $S(x_i, y_i, \hat{y})$ in the observed data.

CP has undergone tremendous developments in recent years (Barber et al., 2023; Park et al., 2024; Tibshirani et al., 2019; Guha et al., 2024) which mirror its increased applicability to challenging settings (Straitouri et al., 2023; Lu et al., 2022). To name a few, it has been applied for designing uncertainty sets in active learning (Ho & Wechsler, 2008), anomaly detection (Laxhammar & Falkman, 2015; Bates et al., 2021), few-shot learning (Fisch et al., 2021), time series (Chernozhukov et al., 2018; Xu & Xie, 2021; Chernozhukov et al., 2021; Lin et al., 2022; Zaffran et al., 2022), or to infer performance guarantees for statistical learning algorithms (Holland, 2020; Cella & Ryan, 2020); and recently to Large Language Models (Kumar et al., 2023; Quach et al., 2023). We refer to the extensive reviews in (Balasubramanian et al., 2014) for other applications in machine learning.

By design, CP requires the notion of order, as the inclusion of a candidate response depends on its relative ranking to the scores observed previously. Hence, the classical strategies developed so far largely target score functions with univariate outputs. This limits their applicability to multivariate responses, as ranking multivariate scores $S(x, y, \hat{y}) \in \mathbb{R}^d, d \geq 2$ is not as straightforward as ranking univariate scores in \mathbb{R} .

Ordering Vector Distributions using Optimal Transport.

In parallel to these developments, and starting with the seminal reference of (Chernozhukov et al., 2017) and more generally the pioneering work of (Hallin et al., 2021; 2022; 2023), multiple references have explored the possibilities offered by the optimal transport theory to define a meaningful ranking or ordering in a multidimensional space. Simply put, the analog of a rank function computed on the data can be found in the optimal **Brenier** map that transports the data measure to a uniform, symmetric, centered measure of reference in \mathbb{R}^d . As a result, a simple notion of a univariate rank for a vector $z \in \mathbb{R}^d$ can be found by evaluating the distance of the image of z (according to that optimal map) to the origin. This approach ensures that the ordering respects both

^{*}Equal contribution ¹Apple.

Correspondence to: Eugene Ndiaye <e.ndiaye@apple.com>.

the geometry, i.e., the spatial arrangement of the data and its distribution: points closer to the center get lower ranks.

Contributions We propose to leverage recent advances in computational optimal transport (Peyré & Cuturi, 2019), using notably differentiable transport map estimators (Pooladian & Niles-Weed, 2021; Cuturi et al., 2019), and apply such map estimators in the definition of multivariate score functions. More precisely:

- **OT-CP:** We extend conformal prediction techniques to multivariate score functions by leveraging optimal transport ordering, which offers a principled way to define and compute a higher-dimensional quantile and cumulative distribution function. As a result, we obtain distribution-free uncertainty sets that capture the joint behavior of multivariate predictions that enhance the flexibility and scope of conformal predictions.
- We propose a computational approach to this theoretical ansatz using the entropic map (Pooladian & Niles-Weed, 2021) computed from solutions to the Sinkhorn problem (Cuturi, 2013). We prove that our approach preserves the coverage guarantee while being tractable.
- We show the application of **OT-CP** using a recently released benchmark of regression tasks (Dheur et al., 2025).

We acknowledge the concurrent proposal of Thurin et al. (2025), who adopt a similar approach to ours, with, however, a few important practical differences, discussed in more detail in Section 6.

2. Background

2.1. Univariate Conformal Prediction

We recall the basics of conformal prediction based on real-valued score function and refer to the recent tutorials (Shafer & Vovk, 2008; Angelopoulos & Bates, 2021). In the following, we denote $[n] := \{1, \dots, n\}$.

For a real-valued random variable Z , it is common to construct an interval $[a, b]$, within which it is expected to fall, as

$$\mathcal{R}_\alpha = \{z \in \mathbb{R} : F(z) \in [a, b]\} \quad (1)$$

This is based on the probability integral transform that states that the cumulative distribution function F maps variables to uniform distribution, i.e., $\mathbb{P}(F(Z) \in [a, b]) = \mathbb{U}([a, b])$. To guarantee a $(1 - \alpha)$ uncertainty region, it suffices to choose a and b such that $\mathbb{U}([a, b]) \geq 1 - \alpha$ which implies

$$\mathbb{P}(Z \in \mathcal{R}_\alpha) \geq 1 - \alpha. \quad (2)$$

Applying it to a real-valued score $Z = S(X, Y)$ of the prediction model \hat{y} , an uncertainty set for the response of a given a input X can be expressed as

$$\mathcal{R}_\alpha(X) = \{y \in \mathcal{Y} : F \circ S(X, y) \in [a, b]\}. \quad (3)$$

However, this result is typically not directly usable, as the ground-truth distribution F is unknown and must be approximated empirically with F_n using finite samples of data. When the sample size goes to infinity, one expects to recover Equation (2). The following result provides the tool to obtain the finite sample version (Shafer & Vovk, 2008).

Lemma 2.1. *If Z_1, \dots, Z_n, Z be a sequence of real-valued exchangeable random variables, then it holds*

$$F_n(Z) \sim \mathbb{U}\left\{0, \frac{1}{n}, \frac{2}{n}, \dots, 1\right\}$$

$$\mathbb{P}(F_n(Z) \in [a, b]) = \mathbb{U}_{n+1}([a, b]) = \frac{\lfloor nb \rfloor - \lceil na \rceil + 1}{n + 1}.$$

By choosing any a, b such that $\mathbb{U}_{n+1}([a, b]) \geq 1 - \alpha$, Lemma 2.1 guarantees a coverage, that is at least equal to the prescribed level of uncertainty

$$\mathbb{P}(Z \in \mathcal{R}_{\alpha, n}) \geq 1 - \alpha.$$

where, the uncertainty set $\mathcal{R}_{\alpha, n} = \mathcal{R}_\alpha(D_n)$ is defined based on observations $D_n = \{Z_1, \dots, Z_n\}$ as:

$$\mathcal{R}_{\alpha, n} = \{z \in \mathbb{R} : F_n(z) \in [a, b]\}. \quad (4)$$

In short, Equation (4) is an empirical version of Equation (1) based on finite data samples that still preserves the coverage probability $(1 - \alpha)$ and does not depend on the ground-truth distribution of the data.

Given data D_n , a prediction model \hat{y} and a new input X_{n+1} , one can build an uncertainty set for the unobserved output Y_{n+1} by applying it to observed score functions.

Proposition 2.2 (Conformal Prediction Coverage). *Consider $Z_i = S(X_i, Y_i)$ for i in $[n]$ and $Z = S(X_{n+1}, Y_{n+1})$ in Lemma 2.1. The conformal prediction set is defined as*

$$\mathcal{R}_{\alpha, n}(X_{n+1}) = \{y \in \mathcal{Y} : F_n \circ S(X_{n+1}, y) \in [a, b]\}$$

and satisfies a finite sample coverage guarantee

$$\mathbb{P}(Y_{n+1} \in \mathcal{R}_{\alpha, n}(X_{n+1})) \geq 1 - \alpha.$$

The conformal prediction coverage guarantee in Proposition 2.2 holds for the *unknown* ground-truth distribution of the data \mathbb{P} , does not require quantifying the estimation error $|F_n - F|$, and is applicable to any prediction model \hat{y} as long as it treats the data exchangeably, e.g., a pre-trained model independent of D_n .

Leveraging the quantile function $F_n^{-1} = Q_n$, and by setting $a = 0$ and $b = 1 - \alpha$, we have the usual description

$$\mathcal{R}_{\alpha, n}(X_{n+1}) = \{y \in \mathcal{Y} : S(X_{n+1}, y) \leq Q_n(1 - \alpha)\}$$

namely the set of all possible responses whose score rank is smaller or equal to $\lceil(1 - \alpha)(n + 1)\rceil$ compared to the rankings of previously observed scores. For the absolute value difference score function, the CP set corresponds to

$$\mathcal{R}_{\alpha,n}(X_{n+1}) = [\hat{y}(X_{n+1}) \pm Q_n(1 - \alpha)].$$

Center-Outward View Another classical choice is $a = \frac{\alpha}{2}$ and $b = 1 - \frac{\alpha}{2}$. In that case, we have the usual confidence set that corresponds to a range of values that captures the central proportion with $\alpha/2$ of the data lying below $Q(\alpha/2)$ and $\alpha/2$ lying above $Q(1 - \alpha/2)$.

Introducing the center-outward distribution of Z as the function $T = 2F - 1$, the probability integral transform $T(Z)$ is uniform in the unit ball $[-1, 1]$. This ensures a symmetric description of $\mathcal{R}_\alpha = T^{-1}(B(0, 1 - \alpha))$ around a central point such as the median $Q(1/2) = T^{-1}(0)$, with the radius of the ball that corresponds to the desired confidence level of uncertainty. Similarly, we have the empirical center-outward distribution $T_n = 2F_n - 1$ and the center-outward view of the conformal prediction set follows as

$$\mathcal{R}_{\alpha,n}(X_{n+1}) = \{y \in \mathcal{Y} : |T_n \circ S(X_{n+1}, y)| \leq 1 - \alpha\}.$$

If Z follows a probability distribution \mathbb{P} , then the transformation $z \mapsto T(z)$ is mapping the source distribution \mathbb{P} to the uniform distribution \mathbb{U} over a unit ball. In fact, it can be characterized as essentially the unique monotone increasing function such that $T(Z)$ is uniformly distributed.

2.2. Multivariate Conformal Prediction

While many conformal methods exist for univariate prediction, we focus here on those applicable to *multivariate* outputs. As recalled in (Dheur et al., 2025), several alternative conformal prediction approaches have been proposed to tackle multivariate prediction problems. Some of these methods can directly operate using a simple predictor (e.g., a conditional mean) of the response y , while some may require stronger assumptions, such as requiring an estimator of the *joint* probability density function between x and y , or access to a generative model that mimics the *conditional* distribution of y given x (Izbicki et al., 2022; Wang et al., 2022).

We restrict our attention to approaches that make no such assumption, reflecting our modeling choices for **OT-CP**.

M-CP. We will consider the template approach of (Zhou et al., 2024) to use classical CP by aggregating a score function computed on each of the d outputs of the multivariate response. Given a conformity score s_i (to be defined next) for the i -th dimension, Zhou et al. (2024) define the following aggregation rule:

$$s_{\text{M-CP}}(x, y) = \max_{i \in [d]} s_i(x, y_i). \quad (5)$$

As (Dheur et al., 2025), we will use *conformalized quantile regression* (Romano et al., 2019) to define the score functions above, for each output $i \in [d]$, where the conformity score is given by:

$$s_i(x, y_i) = \max\{\hat{l}_i(x) - y_i, y_i - \hat{u}_i(x)\},$$

with $\hat{l}_i(x)$ and $\hat{u}_i(x)$ representing the lower and upper conditional quantiles of $Y_i|X = x$ at levels α_l and α_u , respectively. In our experiments, we consider equal-tailed prediction intervals, where $\alpha_l = \frac{\alpha}{2}$, $\alpha_u = 1 - \frac{\alpha}{2}$, and α denotes the miscoverage level.

Merge-CP. An alternative approach is simply to use a squared Euclidean aggregation,

$$s(x, y) := \|\hat{y}(x) - y\|_2,$$

where the choice of the norm (e.g., ℓ_1 , ℓ_2 , or ℓ_∞) depends on the desired sensitivity to errors across tasks. This approach reduces the multidimensional residual to a scalar conformity score, leveraging the natural ordering of real numbers. This simplification not only makes it straightforward to apply univariate conformal prediction methods, but also avoids the complexities of directly managing vector-valued scores in conformal prediction. A variant consists of applying a Mahalanobis norm (Johnstone & Cox, 2021) in lieu of the squared Euclidean norm, using the covariance matrix Σ estimated from the training data (Johnstone & Cox, 2021; Katsios & Papadopoulos, 2024; Henderson et al., 2024),

$$s(x, y) := \|\Sigma^{-1/2}(\hat{y}(x) - y)\|_2,$$

2.3. Kantorovich Ranks

A naive way to define ranks in multiple dimensions might be to measure how far each point is from the origin and then rank them by that distance. This breaks down if the distribution of the data is stretched or skewed in certain directions. To correct for this, Hallin et al. (2021) developed a formal framework of center-outward distributions and quantiles, also called Kantorovich ranks (Chernozhukov et al., 2017), extending the familiar univariate concepts of ranks and quantiles into higher dimensions by building on elements of optimal transport theory.

Optimal Transport Map. Let μ and ν be source and target probability measures on $\Omega \subset \mathbb{R}^d$. One can look for a map $T : \Omega \rightarrow \Omega$ that pushes forward μ to ν and minimizes the average transportation cost

$$T^* \in \arg \min_{T \# \mu = \nu} \int_{\Omega} \|x - T(x)\|^2 d\mu(x). \quad (6)$$

Brenier's theorem states that if the source measure μ has a density, there exists a solution to (6) that is the gradient of a convex function $\phi : \Omega \rightarrow \mathbb{R}$ such that $T^* = \nabla \phi$.

In the one-dimensional case, the cumulative distribution function of a distribution \mathbb{P} is the unique increasing function transporting it to the uniform distribution. This monotonicity property generalizes to higher dimensions through the gradient of a convex function $\nabla\phi$. Thus, one may view the optimal transport map in higher dimensions as a natural analog of the univariate cumulative distribution function: both represent a unique, monotone way to send one probability distribution onto another.

Definition 2.3. The center-outward distribution of a random variable $Z \sim \mathbb{P}$ is defined as the optimal transport map $T = \nabla\phi$ that pushes \mathbb{P} forward to the uniform distribution \mathbb{U} on the unit ball $B(0, 1)$. The rank of Z is defined as $\text{Rank}(Z) = \|T(Z)\|$, the distance from the origin.

Quantile region is an extension of quantiles to multiple dimensions to represent region in the sample space that contains a given proportion of probability mass. The quantile region at probability level $(1 - \alpha) \in (0, 1)$ can be defined as

$$\mathcal{R}_\alpha = \{z \in \mathbb{R}^d : \|T(z)\| \leq 1 - \alpha\}.$$

By definition of the spherical uniform distribution, we have $\|T(Z)\|$ is uniform on $(0, 1)$ which implies

$$\mathbb{P}(Z \in \mathcal{R}_\alpha) = 1 - \alpha. \quad (7)$$

2.4. Entropic Map.

A convenient estimator to approximate the Brenier map T^* from samples (z_1, \dots, z_n) and (u_1, \dots, u_m) is the entropic map (Pooladian & Niles-Weed, 2021): Let $\varepsilon > 0$ and write $K_{ij} = [\exp(-\|z_i - u_j\|^2/\varepsilon)]_{ij}$, the kernel matrix. Define,

$$\mathbf{f}^*, \mathbf{g}^* = \underset{\mathbf{f} \in \mathbb{R}^n, \mathbf{g} \in \mathbb{R}^m}{\text{argmax}} \langle \mathbf{f}, \frac{1}{n} \mathbf{1}_n \rangle + \langle \mathbf{g}, \frac{1}{m} \mathbf{1}_m \rangle - \varepsilon \langle e^{\frac{\mathbf{f}}{\varepsilon}}, K e^{\frac{\mathbf{g}}{\varepsilon}} \rangle. \quad (8)$$

The Equation (8) is an unconstrained concave optimization problem known as the regularized OT problem in dual form (Peyré & Cuturi, 2019, Prop. 4.4) and can be solved numerically with the Sinkhorn algorithm (Cuturi, 2013). Equipped with these optimal vectors, one can define the maps, valid out of sample:

$$f_\varepsilon(z) = \min_\varepsilon([\|z - u_j\|^2 - \mathbf{g}_j^*]_j), \quad (9)$$

$$g_\varepsilon(u) = \min_\varepsilon([\|z_i - u\|^2 - \mathbf{f}_i^*]_i), \quad (10)$$

where for a vector \mathbf{u} or arbitrary size s we define the log-sum-exp operator as $\min_\varepsilon(\mathbf{u}) := -\varepsilon \log(\frac{1}{s} \mathbf{1}_s^T e^{-\mathbf{u}/\varepsilon})$. Using the Brenier (1991) theorem, linking potential values to optimal map estimation, one obtains an estimator for T^* :

$$T_\varepsilon(z) := z - \nabla f_\varepsilon(z) = \sum_{j=1}^m p_j(z) u_j, \quad (11)$$

where the weights depend on z as:

$$p_j(z) := \frac{\exp(-(\|z - u_j\|^2 - \mathbf{g}_j^*)/\varepsilon)}{\sum_{k=1}^m \exp(-(\|z - u_k\|^2 - \mathbf{g}_k^*)/\varepsilon)}. \quad (12)$$

Analogously to (12), one can obtain an estimator for the inverse map $(T^*)^{-1}$ as $T_\varepsilon^{\text{inv}}(u) := \sum_{i=1}^n q_i(u) z_i$, with weights $q_i(u)$ arising for a vector u from the Gibbs distribution of the values $[\|z_i - u\|^2 - \mathbf{f}_i^*]_i$

3. Kantorovich Conformal Prediction

3.1. Multi-Output Conformal Prediction

We suppose that \mathbb{P} is only available through a finite samples and consider the *discrete* transport map

$$T_{n+1} : (Z_i)_{i \in [n+1]} \rightarrow (U_i)_{i \in [n+1]}$$

which can be obtained by solving the optimal assignment problem, which seeks to minimize the total transport cost between the empirical distributions \mathbb{P}_{n+1} and \mathbb{U}_{n+1} :

$$T_{n+1} \in \arg \min_{T \in \mathcal{T}} \sum_{i=1}^{n+1} \|Z_i - T(Z_i)\|^2, \quad (13)$$

where \mathcal{T} is the set of bijections mapping the observed sample $(Z_i)_{i \in [n+1]}$ to the target grid $(U_i)_{i \in [n+1]}$.

Definition 3.1. Let $(Z_1, \dots, Z_n, Z_{n+1})$ be a sequence of exchangeable variables in \mathbb{R}^d that follow a common distribution \mathbb{P} . The discrete center-outward distribution T_{n+1} is the transport map pushing forward \mathbb{P}_{n+1} to \mathbb{U}_{n+1} .

Following (Hallin et al., 2021), we begin by constructing the target distribution \mathbb{U}_{n+1} as a discretized version of a spherical uniform distribution. It is defined such that the total number of points $n + 1 = n_R n_S + n_o$, where n_o points are at the origin:

- n_S unit vectors $\mathbf{u}_1, \dots, \mathbf{u}_{n_S}$ are uniform on the sphere.
- n_R radius are regularly spaced as $\left\{ \frac{1}{n_R}, \frac{2}{n_R}, \dots, 1 \right\}$.

The grid discretizes the sphere into layers of concentric shells, with each shell containing n_S equally spaced points along the directions determined by the unit vectors. The discrete spherical uniform distribution places equal mass over each points of the grid, with $n_o/(n + 1)$ mass on the origin and $1/(n + 1)$ on the remaining points. This ensures isotropic sampling at fixed radius onto $[0, 1]$.

By definition of target distribution \mathbb{U}_{n+1} , it holds

$$\|T_{n+1}(Z_{n+1})\| \sim \mathbb{U}_{n+1} \left\{ 0, \frac{1}{n_R}, \frac{2}{n_R}, \dots, 1 \right\}. \quad (14)$$

In order to define an empirical quantile region as Equation (7), we need an extrapolation \bar{T}_{n+1} of T_{n+1} out of the samples $(Z_i)_{i \in [n+1]}$. By definition of such maps

$$\|\bar{T}_{n+1}(Z_{n+1})\| = \|T_{n+1}(Z_{n+1})\|$$

is still uniformly distributed. With an appropriate choice of radius $r_{\alpha, n+1}$, the empirical quantile region can be defined

$$\mathcal{R}_{\alpha, n+1} = \{z \in \mathbb{R}^d : \|\bar{T}_{n+1}(z)\| \leq r_{\alpha, n+1}\}.$$

When working with such finite samples Z_1, \dots, Z_n, Z_{n+1} , and considering the asymptotic regime (Chewi et al., 2024; Hallin et al., 2021), the empirical source distribution \mathbb{P}_{n+1} converges to the true distribution \mathbb{P} and the empirical transport map \bar{T}_{n+1} converges to the true transport map T^* . As such, with the choice $r_{\alpha, n+1} = 1 - \alpha$, one can expect that $\mathbb{P}(Z \in \mathcal{R}_{\alpha, n+1}) \approx 1 - \alpha$ when n is large.

However, the core point of conformal prediction methodology is to go beyond asymptotic results or regularity assumptions about the data distribution. The following result show how to select a radius preserving the coverage with respect to the ground-truth distribution such as in Equation (18).

Proposition 3.2. *Given n discrete sample points distributed over a sphere with radius $\{0, \frac{1}{n_R}, \frac{2}{n_R}, \dots, 1\}$ and directions uniformly sampled on the sphere, the smallest radius to obtain a coverage $(1 - \alpha)$ is determined by*

$$r_{\alpha, n+1} = \frac{j_\alpha}{n_R} \text{ where } j_\alpha = \left\lceil \frac{(n+1)(1-\alpha) - n_o}{n_S} \right\rceil,$$

where n_S is the number of directions, n_R is the number of radius, and n_o is the number of copies of the origin.

The corresponding conformal prediction set is obtained as:

$$\{y \in \mathcal{Y} : \|\bar{T}_{n+1} \circ S(X_{n+1}, y)\| \leq r_{\alpha, n+1}\}. \quad (15)$$

Remark 3.3 (Computational Issues). While appealing, the previous result has notable computational limitations. At every new candidate $y \in \mathcal{Y}$, the empirical transport map must be recomputed which might be untractable. Moreover, the coverage guarantee does not hold if the transport map is computed solely on a hold-out independent dataset, as it is usually done in split conformal prediction. Plus, for computational efficiency, the empirical entropic map cannot be directly leveraged, since the target values would no longer follow a uniform distribution, as described in Equation (14).

To address these challenges, we propose two simple approaches in the following section.

3.2. Optimal Transport Merging

We introduce optimal transport merging, a procedure that reduces any vector-valued score $S(x, y) \in \mathbb{R}^d$ to a suitable

1D score using OT. We redefine the non-conformity score function of an observation as

$$S_{\text{OT-CP}}(x, y) = \|T^* \circ S(x, y)\| \quad (16)$$

where T^* is the optimal Brenier (1991) map that pushes the distribution of vector-valued scores onto a uniform ball distribution \mathbb{U} of the same dimension. This approach ultimately relies on the natural ordering of the real line, making it possible to directly apply one-dimensional conformal prediction methods to the sequence of transformed scores

$$Z_i = \|S_{\text{OT-CP}}(X_i, Y_i)\| \text{ for } i \in [n+1].$$

In practice, T^* can be replaced by any approximation \hat{T} that preserves the permutation invariance of the score function. The resulting conformal prediction set, **OT-CP** is

$$\mathcal{R}_{\text{OT-CP}}(X_{n+1}, \alpha) = \mathcal{R}_\alpha(\hat{T}, X_{n+1})$$

with respect to a given transport map \hat{T} , and where

$$\mathcal{R}_\alpha(\hat{T}, x) = \{y \in \mathcal{Y} : F_n(\|S_{\text{OT-CP}}(x, y)\|_2) \leq 1 - \alpha\}.$$

have a coverage $(1 - \alpha)$, where F_n is empirical (univariate) cumulative distribution function of the observed scores

$$\{\|S_{\text{OT-CP}}(X_1, Y_1)\|, \dots, \|S_{\text{OT-CP}}(X_n, Y_n)\|\}.$$

Proposition 2.2 directly implies

$$\mathbb{P}(Y_{n+1} \in \mathcal{R}_{\text{OT-CP}}(X_{n+1})) \geq 1 - \alpha.$$

Remark 3.4. Our proposed conformal prediction framework **OT-CP** with optimal transport merging score function generalizes the **Merge-CP** approaches. More specifically, under the additional assumption that we are transporting a source Gaussian (resp. uniform) distribution to a target Gaussian (resp. uniform) distribution, the transport map is affine (Gelbrich, 1990; Muzellec & Cuturi, 2018) with a positive definite linear map term. This results in Equation (16) being equivalent to the Mahalanobis distance.

3.3. Coverage Guarantees under Approximations

When dealing with high-dimensional data or complex distributions, it is essential to find computationally feasible methods to approximate the optimal transport map T^* with a map \hat{T} . In practical applications, we will rely on empirical approximations of the Brenier (1991) map using finite samples. Note that this approach may encounter a few statistical roadblocks, as such estimators are significantly hindered by the curse of dimensionality (Chewi et al., 2024). However, conformal prediction allows us to maintain a coverage level irrespective of sample size limitations. We defer the presentation of this practical approach to section 3.4 and focus first on coverage guarantees.

Coverages of Approximated Quantile Region

Let us assume an arbitrary approximation \hat{T} of the Brenier (1991) map and define the corresponding quantile region as

$$\mathcal{R}(\hat{T}, r) = \{z \in \mathbb{R}^d : \|\hat{T}(z)\| \leq r\},$$

The coverage in Equation (18) is not automatically maintained since $\hat{\mathbb{U}} := \hat{T}_{\#}\mathbb{P}$ may not coincide with \mathbb{U} . As a result, the validity of the approximated quantile region may be compromised unless we can control the magnitude of the error $\|\hat{\mathbb{U}} - \mathbb{U}\|$, which requires additional regularity assumptions. In its standard formulation, conformal prediction relies on an empirical setting and does not directly apply to the continuous case, and hence does not provide a solution for calibrating entropic quantile regions. However, a careful inspection of the 1D case reveals that understanding the distribution of the probability integral transform is key:

$$\bullet \mathbb{U}(\{0, \frac{1}{n}, \frac{1}{2}, \dots, 1\}) \sim F_n(Z) \neq F(Z) \sim \mathbb{U}(0, 1).$$

Instead of relying on an analysis of approximation error to quantify the deviation $|F_n - F|$ under certain regularity conditions, conformal prediction fully characterizes the distribution of the probability integral transform and calibrates the radius of the quantile region accordingly. We follow this idea and note that by definition, we have

$$\mathbb{P}(\mathcal{R}(\hat{T}, r)) = \mathbb{P}(\|\hat{T}(z)\| \leq r) = \hat{\mathbb{U}}(B(0, r)).$$

Instead of relying on $\hat{\mathbb{U}} \approx \mathbb{U}$, we define

$$r_\alpha(\hat{T}, \mathbb{P}) = \inf\{r : \hat{\mathbb{U}}(B(0, r)) \geq 1 - \alpha\} \quad (17)$$

that naturally leads to a desired coverage with the approximated transported map. For $\hat{r}_\alpha = r_\alpha(\hat{T}, \mathbb{P})$, it holds

$$\mathbb{P}(Z \in \mathcal{R}(\hat{T}, \hat{r}_\alpha)) \geq 1 - \alpha.$$

By extension, a quantile region of the vector-valued score $Z = S(X, Y) \in \mathbb{R}^d$ of a prediction model \hat{y} provides an uncertainty set for the response of a given input X , with the prescribed coverage $(1 - \alpha)$ expressed as

$$\begin{aligned} \hat{\mathcal{R}}_\alpha(X) &= \{y \in \mathcal{Y} : \|\hat{T} \circ S(X, y)\| \leq \hat{r}_\alpha\}. \\ \mathbb{P}(Y \in \hat{\mathcal{R}}_\alpha(X)) &\geq 1 - \alpha. \end{aligned} \quad (18)$$

We give the finite sample analogy of Equation (18), which provides a coverage guarantee even when the transport map is an approximation obtained using both entropic regularization and finite sample data e.g in Equation (11). Given such an approximated map \hat{T}_{n+1} and applying and the empirical radius $\hat{r}_{\alpha, n+1} = r_\alpha(\hat{T}_{n+1}, \mathbb{P}_{n+1})$, it holds

$$\mathbb{P}_{n+1}(Z_{n+1} \in \mathcal{R}(\hat{T}_{n+1}, \hat{r}_{\alpha, n+1})) \geq 1 - \alpha.$$

However, this is *only* an empirical coverage statement:

$$\frac{1}{n+1} \sum_{i=1}^{n+1} \mathbb{1}\{Z_i \in \mathcal{R}(\hat{T}_{n+1}, \hat{r}_{\alpha, n+1})\} \geq 1 - \alpha$$

which does not imply coverage wrt \mathbb{P} unless $n \rightarrow \infty$. The following result shows how to obtain finite sample validity.

Lemma 3.5 (Coverage of Empirical Quantile Region). *Let Z_1, \dots, Z_n, Z_{n+1} be a sequence of exchangeable variables in \mathbb{R}^d , then, $\mathbb{P}(Z_{n+1} \in \hat{\mathcal{R}}_{\alpha, n+1}) \geq 1 - \alpha$, where, for simplicity, we denoted the approximated empirical quantile region as $\hat{\mathcal{R}}_{\alpha, n+1} = \mathcal{R}(\hat{T}_{n+1}, \hat{r}_{\alpha, n+1})$.*

This can be directly applied to obtain conformal prediction set for vector-valued non-conformity score functions $Z_i = S(X_i, Y_i) \in \mathbb{R}^d$ for i in $[n+1]$ in Lemma 3.5.

Proposition 3.6. *The conformal prediction set is defined as*

$$\hat{\mathcal{R}}_{\alpha, n+1}(X_{n+1}) = \{y \in \mathcal{Y} : \|\hat{T} \circ S(X_{n+1}, y)\| \leq \hat{r}_{\alpha, n+1}\}$$

with $\hat{r}_{\alpha, n+1} = \inf\{r \geq 0 : \hat{\mathbb{U}}_{n+1}(B(0, r)) \geq 1 - \alpha\}$. It satisfies a distribution-free finite sample coverage guarantee

$$\mathbb{P}(Y_{n+1} \in \hat{\mathcal{R}}_{\alpha, n+1}(X_{n+1})) \geq 1 - \alpha. \quad (19)$$

Approaches relying on vector-valued probability integral transform, e.g., by leveraging Copulas, have been recently explored (Messoudi et al., 2021; Park et al., 2024) and concluded that loss of coverage can occur when the estimated copula of the scores deviates from the true copula and thus does not formally guarantee finite-sample validity. To our knowledge, Proposition 3.6 provides the first calibration guarantee for such confidence regions without assumptions on the distribution, for any approximation map \hat{T} .

3.4. Implementation with the Entropic Map

We assume access to two families of samples: residuals (z_1, \dots, z_n) , and a discretization of the uniform grid on the sphere, (u_1, \dots, u_m) , with sizes n, m that will be usually different, $n \neq m$. Learning the entropic map estimator as in Section 3.4 requires running the Sinkhorn (1964) algorithm for a given regularization ε on a $n \times m$ cost matrix. At test time, for each evaluation, computing the weights in Equation (12) requires computing the distances of a new score z to the uniform grid. The complexity is therefore $O(nm)$ when training the map and conformalizing its norms, and $O(m)$ to transport a conformity score for a given y .

Sampling on the sphere. As mentioned by Hallin et al. (2021), it is preferable to sample the uniform measure \mathbb{U}_d with diverse samples. This can be achieved using stratified sampling on radii lengths and low-discrepancy samples picked on the sphere. We borrow inspiration from

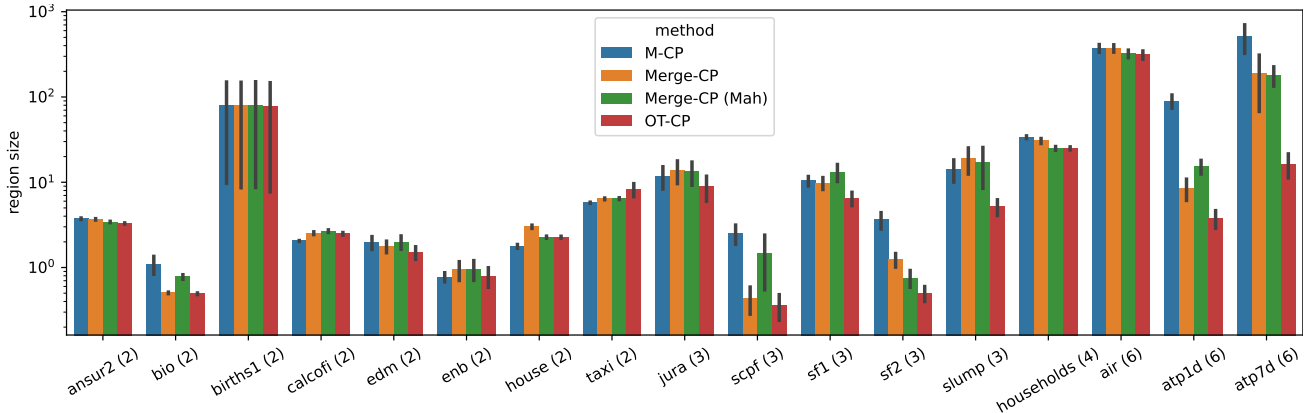


Figure 1. We report the mean and standard error of the region size across 10 different seeds. For **M-CP**, we use 300 samples to compute the conditional mean, and for **OT-CP**, we use $\varepsilon = 0.1$ and $2^{15} = 32768$ points in the uniform target measure. Overall, **OT-CP** displays smaller region size than other baselines (13 out of 17 datasets). The output dimension d of each dataset is provided next to its name.

the review provided in (Nguyen et al., 2024) and pick their *Gaussian based* mapping approach (Basu, 2016). This consists of mapping a low-discrepancy sequence w_1, \dots, w_L on $[0, 1]^d$ to a potentially low-discrepancy sequence $\theta_1, \dots, \theta_L$ on \mathbb{S}^{d-1} through the mapping $\theta = \Phi^{-1}(w) / \|\Phi^{-1}(w)\|_2$, where Φ^{-1} is the inverse CDF of $\mathcal{N}(0, 1)$ applied entry-wise.

4. Experiments

4.1. Setup and Metrics

We borrow the experimental setting provided by Dheur et al. (2025) and benchmark multivariate conformal methods on a total of 24 tabular datasets. Total data size n in these datasets ranges from 103 to 50,000, with input dimension p ranging from 1 to 348, and output dimension d ranging from 2 to 16. We adopt their approach, which is to rely on a multivariate quantile function forecaster (MQF², Kan et al., 2022), a normalizing flow that is able to quantify output uncertainty conditioned on input x . However, in accordance with our stance mentioned in the background section, we will only assume access to the conditional mean (point-wise) estimator for **OT-CP**.

As is common in the field, we evaluate the methods using several metrics, including marginal coverage (MC), and mean region size (Size). The latter is using importance sampling, leveraging (when computing test time metrics only), the generative flexibility provided by the MQF² as an invertible flow. See (Dheur et al., 2025) and their code for more details on the experimental setup.

4.2. Hyperparameter Choices

We apply default parameters for all three competing methods, **M-CP** and **Merge-CP**, using (or not) the Mahalanobis correction. For **M-CP** using conformalized quantile regres-

sion boxes, we follow (Dheur et al., 2025) and leverage the empirical quantiles return by MQF² to compute boxes (Zhou et al., 2024).

OT-CP: our implementation requires tuning two important hyperparameters: the entropic regularization ε and the total number of points used to discretize the sphere m , not necessarily equal to the input data sample size n . These two parameters describe a fundamental statistical and computational trade-off. On the one hand, it is known that increasing m will mechanically improve the ability of T_ε to recover in the limit T^* (or at least solve the semi-discrete (Peyré & Cuturi, 2019) problem of mapping n data points to the sphere). However, large m incurs a heavier computational price when running the Sinkhorn algorithm. On the other hand, increasing ε improves on *both* computational and statistical aspects, but deviates further the estimated map from the ground truth T^* to target instead a blurred map. We have experimented with these aspects and derive from our experiments that both m and ε should be increased to track increase in dimension. As a sidenote, we do observe that debiasing the outputs of the Sinkhorn algorithm does not result in improved results, which agrees with the findings in (Pooladian et al., 2022). We use the OTT-JAX toolbox (Cuturi et al., 2022) to compute these maps.

4.3. Results

We present results by differentiating datasets with small dimension $d \leq 6$ from datasets with higher dimensionality $14 \leq d \leq 16$, that we expect to be more challenging to handle with OT approaches, owing to the curse of dimensionality that might degrade the quality of multivariate quantiles. Results in Figure 4 indicate an improvement (smaller region for similar coverage) on 15 out of 18 datasets in lower dimensions, this edge vanishing in the higher-dimensional regime. Ablations provided in Figure 2 highlight the role of

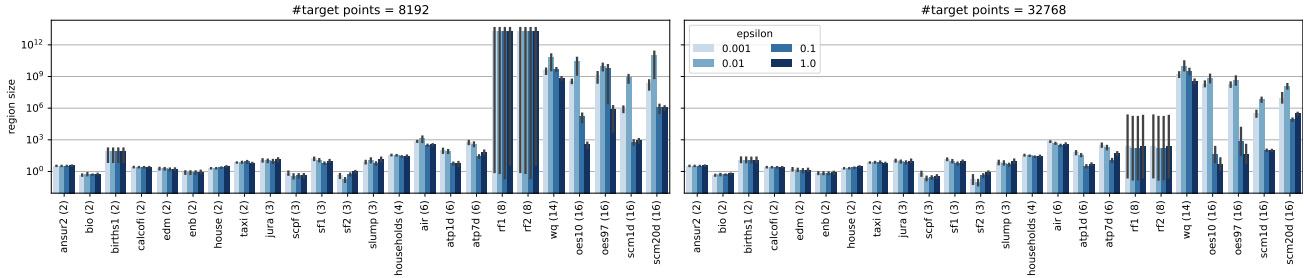


Figure 2. This plot details the impact of the two important hyperparameters one needs to set in **OT-CP**: number of target points m sampled from the uniform ball and the ϵ regularization level. As can be seen, larger sample size m improves region size (smaller the better) for roughly all datasets and regularization strengths. On the other hand, one must tune ϵ to operate at a suitable regime: not too low, which results in the well-documented poor statistical performance of unregularized / linear program OT, nor too high, which would lead to a collapse of the entropic map to the sphere. Using **OTT-JAX** and its automatic normalizations, we see that $\epsilon = 0.1$ works best overall.

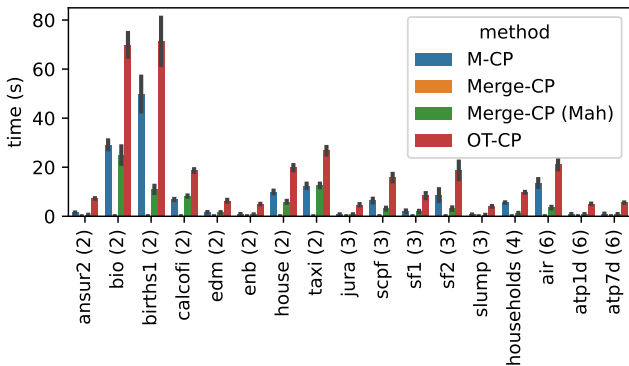


Figure 3. Computational time on small dimensional datasets. **OT-CP** incurs more compute time due to the OT map estimation. See Fig.7 for a similar picture for higher dimensional datasets.

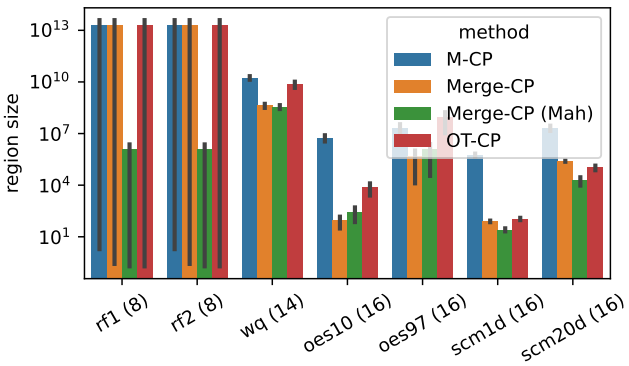


Figure 4. As in 1, we report mean and standard errors for region size (log scale) across 10 different seeds for larger datasets. We keep the same parameters and importantly $\epsilon = 0.1$ and $2^{15} = 32768$ points in the uniform target measure. We expect the performance of **OT-CP** to decrease with dimensionality, but it does provide a convincing alternative to the other approaches.

ϵ and m , the entropic regularization strength and the sphere size respectively. These results show that results for high m tend to be better but more costly, while the tuning of the regularization strength ϵ needs to be tuned according to dimension (Vacher & Vialard, 2022). Finally, Figure 5 provides an illustration of the non-elliptic CP regions outputted by **OT-CP**, by pulling back the rescaled uniform sphere using the inverse entropic mapping described in Section 3.4.

5. Conclusion

We have proposed **OT-CP**, a new approach that can leverage a recently proposed formulation for multivariate quantiles that uses optimal transport theory and optimal transport map estimators. We show the theoretical soundness of this approach, but, most importantly, demonstrate its applicability throughout a broad range of tasks compiled by (Dheur et al., 2025). Compared to similar baselines that either use a conditional mean regression estimator (**Merge-CP**), or more involved quantile regression estimators (**M-CP**), **OT-CP** shows overall superior performance, while incurring, predictably, a higher train / calibration time cost. The chal-

lenges brought forward by the estimation of OT maps in high dimensions (Chewi et al., 2024) require being particularly careful when tuning entropic regularization and grid size. However, we show that there exists a reasonable setting for both of these parameters that delivers good performance across most tasks.

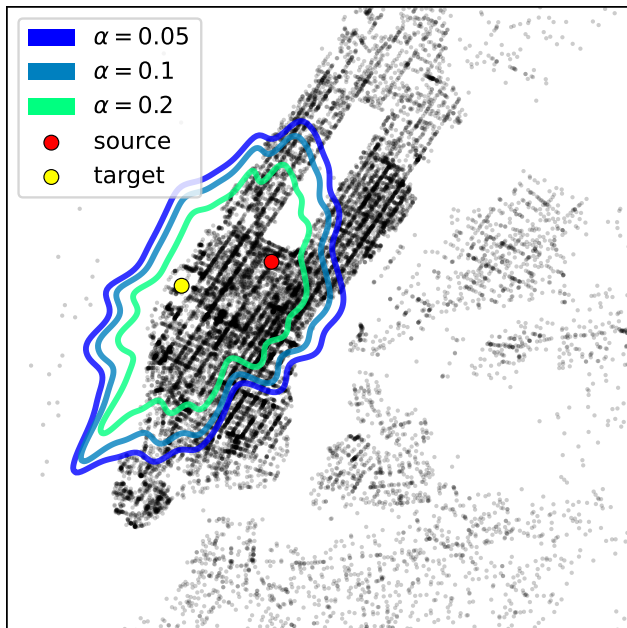


Figure 5. Conformal sets recovered by mapping back the reduced sphere on the Manhattan map, in agreement with Equation 18, on a prediction for the `taxi` dataset. We use the inverse entropic map mentioned in Section 3.4, mapping back the gridded sphere of size $m = 2^{15}$ for each level, and plotting its outer contour.

6. Concurrent Work.

Concurrently to our work, Thurin et al. (2025) proposed recently to leverage OT in CP with a similar approach, deriving a similar CP set as in Equation (15) and analyzing a variant with asymptotic conditional coverage under additional regularity assumptions. However, our methods differ in several key aspects. On the computational side, our implementation leverages general entropic maps (Section 3.4) without compromising finite-sample coverage guarantees, an aspect we analyze in detail in Section 3.3. In contrast, their approach requires solving a linear assignment problem, using for instance the Hungarian algorithm, which has cubic complexity $O(n^3)$ in the number of target points, and which also requires having a target set on the sphere that is of the same size as the number of input points. With our notations in Section 3.4, they require $n = m$, whereas we set m to anywhere between 2^{12} and 2^{15} , independently of n . While they mention efficient approximations that reduce complexity to quadratic in (Thurin et al., 2025, Remark 2.3), their theoretical results do not yet cover these cases since their analysis relies on the fact that ranks are random permutations of $\{1/n, 2/n, \dots, 1\}$, which cannot be extended to using Sinkhorn with soft assignment. In contrast, our work establishes formal theoretical coverage guarantees even when approximated (pre-trained) transport map are used.

References

- Angelopoulos, A. N. and Bates, S. A gentle introduction to conformal prediction and distribution-free uncertainty quantification. *arXiv preprint arXiv:2107.07511*, 2021.
- Balasubramanian, V., Ho, S.-S., and Vovk, V. *Conformal prediction for reliable machine learning: theory, adaptations and applications*. Newnes, 2014.
- Barber, R. F., Candès, E. J., Ramdas, A., and Tibshirani, R. J. Conformal prediction beyond exchangeability. *The Annals of Statistics*, 51(2):816–845, 2023.
- Basu, K. *Quasi-Monte Carlo Methods in Non-Cubical Spaces*. Stanford University, 2016.
- Bates, S., Candès, E., Lei, L., Romano, Y., and Sesia, M. Testing for outliers with conformal p-values. *arXiv preprint arXiv:2104.08279*, 2021.
- Brenier, Y. Polar factorization and monotone rearrangement of vector-valued functions. *Communications on Pure and Applied Mathematics*, 44(4), 1991. doi: 10.1002/cpa.3160440402.
- Cella, L. and Ryan, R. Valid distribution-free inferential models for prediction. *arXiv preprint arXiv:2001.09225*, 2020.
- Chernozhukov, V., Galichon, A., Hallin, M., and Henry, M. Monge–Kantorovich depth, quantiles, ranks and signs. *The Annals of Statistics*, 45(1):223 – 256, 2017. doi: 10.1214/16-AOS1450. URL <https://doi.org/10.1214/16-AOS1450>.
- Chernozhukov, V., Wüthrich, K., and Zhu, Y. Exact and robust conformal inference methods for predictive machine learning with dependent data. *Conference On Learning Theory*, 2018.
- Chernozhukov, V., Wüthrich, K., and Zhu, Y. An exact and robust conformal inference method for counterfactual and synthetic controls. *Journal of the American Statistical Association*, 116(536):1849–1864, 2021.
- Chewi, S., Niles-Weed, J., and Rigollet, P. Statistical optimal transport. *arXiv preprint arXiv:2407.18163*, 2024.
- Cuturi, M. Sinkhorn distances: Lightspeed computation of optimal transport. In *Advances in neural information processing systems*, pp. 2292–2300, 2013.
- Cuturi, M., Teboul, O., and Vert, J.-P. Differentiable ranking and sorting using optimal transport. *Advances in neural information processing systems*, 32, 2019.

- Cuturi, M., Meng-Papaxanthos, L., Tian, Y., Bunne, C., Davis, G., and Teboul, O. Optimal transport tools (ott): A jax toolbox for all things wasserstein, 2022. URL <https://arxiv.org/abs/2201.12324>.
- Dheur, V., Fontana, M., Estievenart, Y., Desobry, N., and Taieb, S. B. Multi-output conformal regression: A unified comparative study with new conformity scores, 2025. URL <https://arxiv.org/abs/2501.10533>.
- Fisch, A., Schuster, T., Jaakkola, T., and Barzilay, R. Few-shot conformal prediction with auxiliary tasks. *ICML*, 2021.
- Gamerman, A., Vovk, V., and Vapnik, V. Learning by transduction, 1998.
- Gelbrich, M. On a formula for the l^2 wasserstein metric between measures on euclidean and hilbert spaces. *Mathematische Nachrichten*, 147(1), 1990.
- Guha, E., Natarajan, S., Möllenhoff, T., Khan, M. E., and Ndiaye, E. Conformal prediction via regression-as-classification. *arXiv preprint arXiv:2404.08168*, 2024.
- Hallin, M., del Barrio, E., Cuesta-Albertos, J., and Matrán, C. Distribution and quantile functions, ranks and signs in dimension d : A measure transportation approach. *The Annals of Statistics*, 49(2):1139 – 1165, 2021. doi: 10.1214/20-AOS1996. URL <https://doi.org/10.1214/20-AOS1996>.
- Hallin, M., La Vecchia, D., and Liu, H. Center-outward r -estimation for semiparametric varma models. *Journal of the American Statistical Association*, 117(538):925–938, 2022.
- Hallin, M., Hlubinka, D., and Hudecová, Š. Efficient fully distribution-free center-outward rank tests for multiple-output regression and manova. *Journal of the American Statistical Association*, 118(543):1923–1939, 2023.
- Henderson, I., Mazoyer, A., and Gamboa, F. Adaptive inference with random ellipsoids through conformal conditional linear expectation. *arXiv preprint arXiv:2409.18508*, 2024.
- Ho, S.-S. and Wechsler, H. Query by transduction. *IEEE transactions on pattern analysis and machine intelligence*, 2008.
- Holland, M. J. Making learning more transparent using conformalized performance prediction. *arXiv preprint arXiv:2007.04486*, 2020.
- Izbicki, R., Shimizu, G., and Stern, R. B. Cd-split and hpd-split: Efficient conformal regions in high dimensions. *Journal of Machine Learning Research*, 23(87): 1–32, 2022.
- Johnstone, C. and Cox, B. Conformal uncertainty sets for robust optimization. In Carlsson, L., Luo, Z., Cherubin, G., and An Nguyen, K. (eds.), *Proceedings of the Tenth Symposium on Conformal and Probabilistic Prediction and Applications*, volume 152 of *Proceedings of Machine Learning Research*, pp. 72–90. PMLR, 08–10 Sep 2021. URL <https://proceedings.mlr.press/v152/johnstone21a.html>.
- Kan, K., Aubet, F.-X., Januschowski, T., Park, Y., Benidis, K., Ruthotto, L., and Gasthaus, J. Multivariate quantile function forecaster. In *International Conference on Artificial Intelligence and Statistics*, pp. 10603–10621. PMLR, 2022.
- Katsios, K. and Papadopoulos, H. Multi-label conformal prediction with a mahalanobis distance nonconformity measure. In Vantini, S., Fontana, M., Solari, A., Boström, H., and Carlsson, L. (eds.), *Proceedings of the Thirteenth Symposium on Conformal and Probabilistic Prediction with Applications*, volume 230 of *Proceedings of Machine Learning Research*, pp. 522–535. PMLR, 09–11 Sep 2024. URL <https://proceedings.mlr.press/v230/katsios24a.html>.
- Kumar, B., Lu, C., Gupta, G., Palepu, A., Bellamy, D., Raskar, R., and Beam, A. Conformal prediction with large language models for multi-choice question answering. *arXiv preprint arXiv:2305.18404*, 2023.
- Laxhammar, R. and Falkman, G. Inductive conformal anomaly detection for sequential detection of anomalous sub-trajectories. *Annals of Mathematics and Artificial Intelligence*, 2015.
- Lin, Z., Trivedi, S., and Sun, J. Conformal prediction intervals with temporal dependence. *Transactions of Machine Learning Research*, 2022.
- Lu, C., Lemay, A., Chang, K., Höbel, K., and Kalpathy-Cramer, J. Fair conformal predictors for applications in medical imaging. In *Proceedings of the AAAI Conference on Artificial Intelligence*, volume 36, pp. 12008–12016, 2022.
- Messoudi, S., Destercke, S., and Rousseau, S. Copula-based conformal prediction for multi-target regression. *Pattern Recognition*, 120:108101, 2021.
- Muzellec, B. and Cuturi, M. Generalizing point embeddings using the wasserstein space of elliptical distributions. *Advances in Neural Information Processing Systems*, 31, 2018.
- Nguyen, K., Bariletto, N., and Ho, N. Quasi-monte carlo for 3d sliced wasserstein. In *The Twelfth International Conference on Learning Representations*, 2024.

- Park, J. W., Tibshirani, R., and Cho, K. Semiparametric conformal prediction. *arXiv preprint arXiv:2411.02114*, 2024.
- Peyré, G. and Cuturi, M. Computational optimal transport. *Foundations and Trends® in Machine Learning*, 11, 2019.
- Pooladian, A.-A. and Niles-Weed, J. Entropic estimation of optimal transport maps. *arXiv preprint arXiv:2109.12004*, 2021.
- Pooladian, A.-A., Cuturi, M., and Niles-Weed, J. Debiasser beware: Pitfalls of centering regularized transport maps. In *International Conference on Machine Learning*, pp. 17830–17847. PMLR, 2022.
- Quach, V., Fisch, A., Schuster, T., Yala, A., Sohn, J. H., Jaakkola, T. S., and Barzilay, R. Conformal language modeling. *arXiv preprint arXiv:2306.10193*, 2023.
- Romano, Y., Patterson, E., and Candes, E. Conformalized quantile regression. *Advances in neural information processing systems*, 32, 2019.
- Shafer, G. and Vovk, V. A tutorial on conformal prediction. *Journal of Machine Learning Research*, 2008.
- Sinkhorn, R. A relationship between arbitrary positive matrices and doubly stochastic matrices. *Ann. Math. Statist.*, 35:876–879, 1964.
- Straitouri, E., Wang, L., Okati, N., and Rodriguez, M. G. Improving expert predictions with conformal prediction. In *International Conference on Machine Learning*, pp. 32633–32653. PMLR, 2023.
- Thurin, G., Nadjahi, K., and Boyer, C. Optimal transport-based conformal prediction, 2025. URL <https://arxiv.org/abs/2501.18991>.
- Tibshirani, R. J., Foygel Barber, R., Candes, E., and Ramdas, A. Conformal prediction under covariate shift. *Advances in neural information processing systems*, 32, 2019.
- Vacher, A. and Vialard, F.-X. Parameter tuning and model selection in optimal transport with semi-dual brenier formulation. In Oh, A. H., Agarwal, A., Belgrave, D., and Cho, K. (eds.), *Advances in Neural Information Processing Systems*, 2022.
- Vovk, V., Gammerman, A., and Shafer, G. *Algorithmic learning in a random world*. Springer, 2005.
- Wang, Z., Gao, R., Yin, M., Zhou, M., and Blei, D. M. Probabilistic conformal prediction using conditional random samples. *arXiv preprint arXiv:2206.06584*, 2022.
- Xu, C. and Xie, Y. Conformal prediction interval for dynamic time-series. *ICML*, 2021.
- Zaffran, M., Féron, O., Goude, Y., Josse, J., and Dieuleveut, A. Adaptive conformal predictions for time series. In *International Conference on Machine Learning*, pp. 25834–25866. PMLR, 2022.
- Zhou, Y., Lindemann, L., and Sesia, M. Conformalized adaptive forecasting of heterogeneous trajectories. *arXiv preprint arXiv:2402.09623*, 2024.

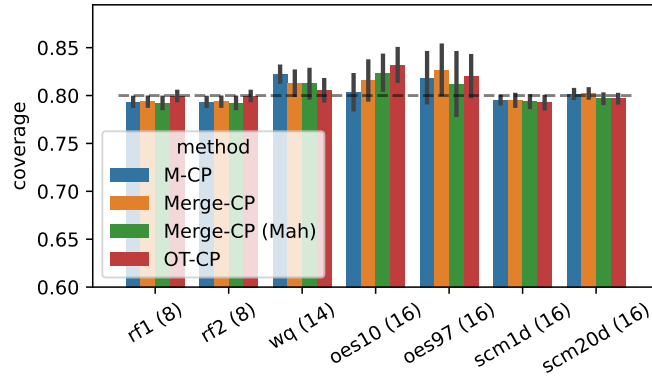


Figure 6. Coverage for higher dimensional datasets, corresponding to the setting displayed in Figure 6.

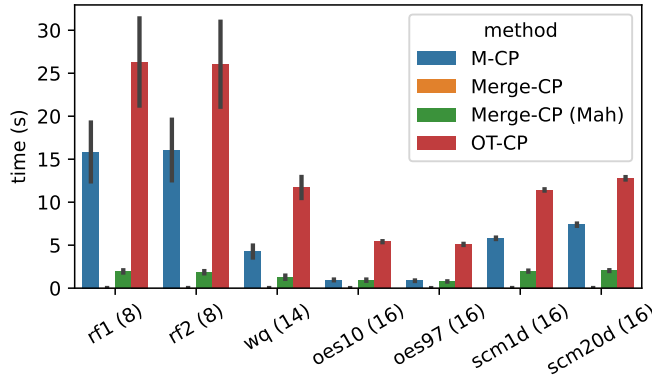


Figure 7. Runtimes for higher dimensional datasets, corresponding to the setting displayed in Figure 6.

A. Appendix

We provide a few additional results related to the experiments proposed in Section 4.

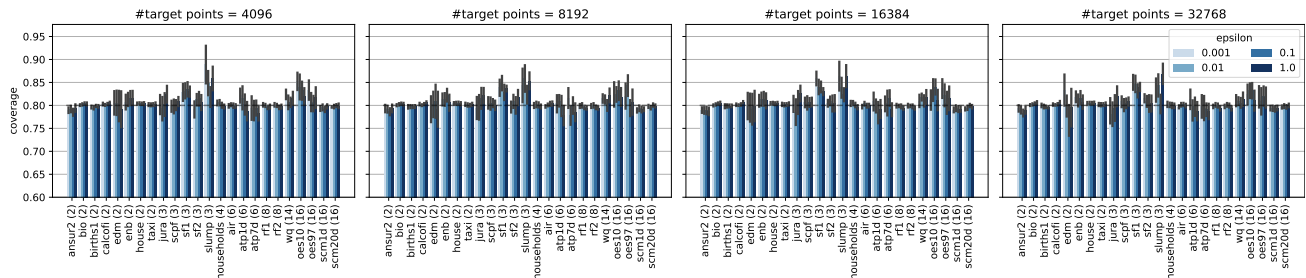


Figure 8. Ablation: coverage quality as a function of hyperparameters, with the setting corresponding to Figure 2.

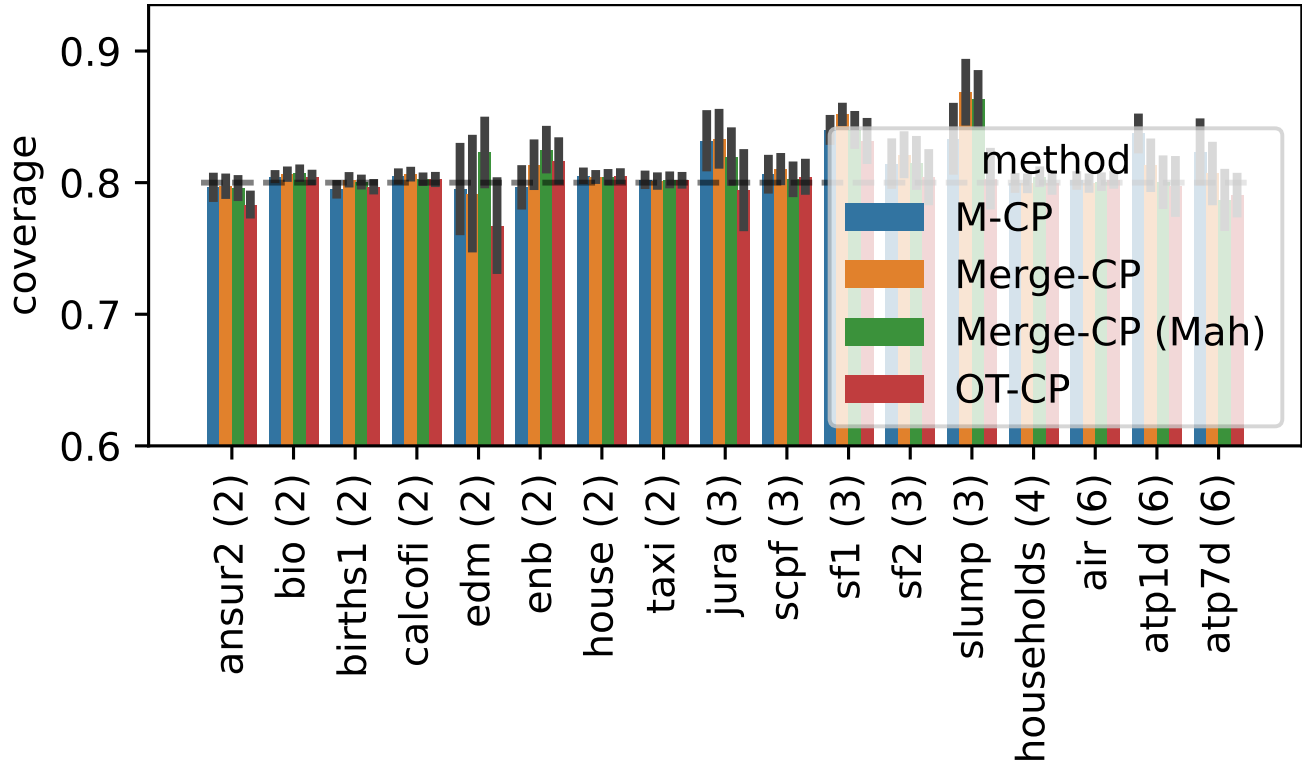


Figure 9. Coverage of all baselines on small dimensional datasets, corresponding to the region sizes given in Figure 1.

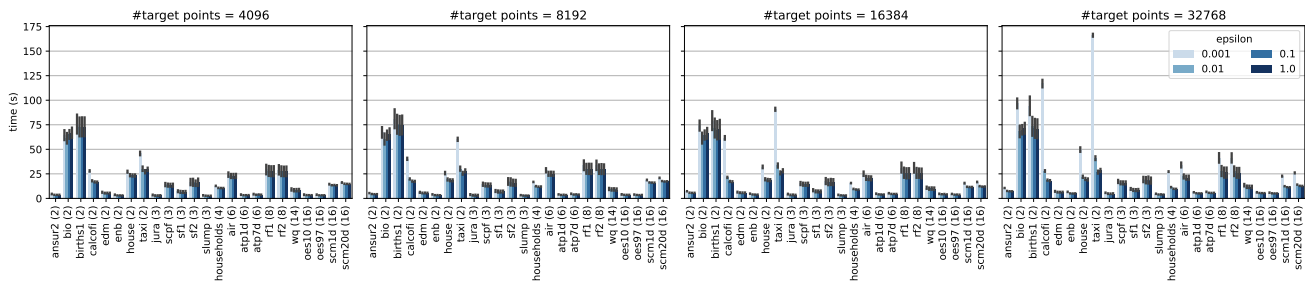


Figure 10. Ablation: running time as a function of hyperparameters, with the setting corresponding to Figure 2.

B. Proofs

Proposition B.1. *Given n discrete sample points distributed over a sphere with radii $\{0, \frac{1}{n_R}, \frac{2}{n_R}, \dots, 1\}$ and directions uniformly sampled on the sphere, the smallest radius $r_\alpha = \frac{j_\alpha}{n_R}$ satisfying $(1 - \alpha)$ -coverage is determined by*

$$j_\alpha = \left\lceil \frac{(n+1)(1-\alpha) - n_o}{n_S} \right\rceil,$$

where n_S is the number of directions, n_R is the number of radii, and n_o is the number of copies of the origin ($\|U\| = 0$).

Proof. The discrete spherical uniform distribution places the same probability mass on all $n+1$ sample points, including the n_o copies of the origin. As such, given a radius $r_j = \frac{j}{n_R}$, we have

$$\mathbb{P}(\|U\| = r_j) = n_S \cdot \frac{1}{n+1}.$$

The cumulative probability up to radius r_j is given by:

$$\mathbb{P}(\|U\| \leq r_j) = \mathbb{P}(\|U\| = 0) + \sum_{k=1}^j \mathbb{P}(\|U\| = r_k) = \frac{n_o}{n+1} + j \times \frac{n_S}{n+1}.$$

To find the smallest $r_\alpha = \frac{j_\alpha}{n_R}$ such that $\mathbb{P}(\|U\| \leq r_{j_\alpha}) \geq 1 - \alpha$, it suffices to solve:

$$\frac{n_o}{n+1} + j_\alpha \times \frac{n_S}{n+1} \geq 1 - \alpha.$$

□

Lemma B.2 (Coverage of Empirical Quantile Region). *Let Z_1, \dots, Z_n, Z_{n+1} be a sequence of exchangeable variables in \mathbb{R}^d , then, $\mathbb{P}(Z_{n+1} \in \widehat{\mathcal{R}}_{\alpha, n+1}) \geq 1 - \alpha$, where, for simplicity, we denoted the approximated empirical quantile region as $\widehat{\mathcal{R}}_{\alpha, n+1} = \mathcal{R}(\widehat{T}_{n+1}, \widehat{r}_{\alpha, n+1})$.*

Proof. By exchangeability of Z_1, \dots, Z_{n+1} and symmetry of the set $\widehat{\mathcal{R}}_{\alpha, n+1}$, it holds

$$\mathbb{P}(Z_{n+1} \in \widehat{\mathcal{R}}_{\alpha, n+1}) = \mathbb{P}(Z_i \in \widehat{\mathcal{R}}_{\alpha, n+1}) \quad \forall i \in [n+1].$$

By taking the average on both side, we have:

$$\begin{aligned} \mathbb{P}(Z_{n+1} \in \widehat{\mathcal{R}}_{\alpha, n+1}) &= \frac{1}{n+1} \sum_{i=1}^{n+1} \mathbb{P}(Z_i \in \widehat{\mathcal{R}}_{\alpha, n+1}) \\ &= \mathbb{E} \left[\frac{1}{n+1} \sum_{i=1}^{n+1} \mathbb{1}\{Z_i \in \widehat{\mathcal{R}}_{\alpha, n+1}\} \right] \\ &= \mathbb{E} \left[\mathbb{P}_{n+1}(Z_{n+1} \in \widehat{\mathcal{R}}_{\alpha, n+1}) \right] \\ &\geq 1 - \alpha. \end{aligned}$$

□

Multivariate Conformal Prediction using Optimal Transport

epsilon	#target	ansur2 (2)	bio (2)	births1 (2)	calcofi (2)	edm (2)	enb (2)	house (2)	taxi (2)	jura (3)	scfp (3)	sf1 (3)	sf2 (3)
0.001	4096	3.3±0.064	0.46±0.057	78±70	2.6±0.089	1.9±0.3	0.81±0.21	2±0.051	7±0.12	13±2.6	0.78±0.4	14±2.6	0.82±0.32
	8192	3.4±0.059	0.45±0.057	78±70	2.6±0.089	1.9±0.29	0.81±0.2	2±0.05	7±0.13	11±2.6	0.73±0.23	16±3.9	0.4±0.16
	16384	3.4±0.059	0.46±0.058	78±70	2.6±0.093	1.8±0.28	0.83±0.21	2±0.048	7±0.13	12±2.3	0.87±0.34	21±4.8	0.44±0.2
	32768	3.4±0.063	0.46±0.058	78±70	2.6±0.092	1.9±0.3	0.81±0.2	2±0.05	7±0.13	12±2.6	1.2±0.47	16±2.9	0.57±0.18
0.01	4096	3.3±0.055	0.55±0.12	78±70	2.5±0.084	1.9±0.3	0.81±0.21	2±0.05	7.5±0.63	11±2.8	0.43±0.15	12±2.1	0.2±0.086
	8192	3.3±0.054	0.56±0.13	78±70	2.5±0.082	1.8±0.3	0.8±0.21	2±0.049	7.5±0.69	10±2.6	0.37±0.15	12±2.8	0.17±0.063
	16384	3.3±0.045	0.56±0.12	78±70	2.5±0.082	1.7±0.24	0.8±0.21	2±0.05	7.5±0.71	13±4.3	0.4±0.18	11±2.9	0.19±0.076
	32768	3.3±0.064	0.56±0.12	78±70	2.5±0.085	1.7±0.26	0.82±0.22	2±0.049	7.5±0.69	10±2.7	0.41±0.17	12±2.6	0.18±0.071
0.1	4096	3.3±0.058	0.49±0.011	78±70	2.5±0.084	1.6±0.25	0.81±0.21	2.3±0.065	8.3±1.4	9.2±2.8	0.37±0.15	6.6±0.96	0.48±0.1
	8192	3.3±0.059	0.49±0.011	78±70	2.5±0.084	1.6±0.26	0.8±0.21	2.3±0.065	8.2±1.5	9.4±2.9	0.4±0.15	6.1±0.89	0.53±0.11
	16384	3.3±0.054	0.49±0.012	78±70	2.5±0.081	1.6±0.26	0.8±0.21	2.3±0.058	8.2±1.4	9.4±2.9	0.37±0.12	6.4±0.83	0.45±0.092
	32768	3.3±0.051	0.49±0.011	77±70	2.5±0.083	1.5±0.25	0.92±0.24	2.3±0.057	8.2±1.4	8.9±2.9	0.36±0.12	6.5±1.2	0.5±0.1
1	4096	3.6±0.055	0.65±0.019	78±70	2.5±0.1	1.7±0.27	0.92±0.24	3±0.13	6.4±0.14	13±4	0.45±0.16	9.5±1.9	0.84±0.13
	8192	3.6±0.067	0.59±0.013	78±70	2.5±0.099	1.7±0.26	0.91±0.24	3±0.14	6.3±0.14	13±4	0.42±0.14	10±1.8	0.93±0.16
	16384	3.5±0.072	0.57±0.016	78±70	2.5±0.099	1.7±0.27	0.91±0.24	3±0.13	6.4±0.14	14±4	0.48±0.17	9.8±1.7	0.91±0.17
	32768	3.5±0.061	0.6±0.028	78±71	2.5±0.1	1.7±0.27	0.91±0.24	2.9±0.13	6.4±0.15	13±4	0.47±0.17	10±1.7	0.9±0.17

epsilon	#target	slump (3)	households (4)	air (6)	atp1d (6)	atp7d (6)
0.001	4096	15±7.6	37±1.4	2.6E+03±1.9E+03	81±19	8.5E+02±4.5E+02
	8192	7.9±2	36±1.9	7.1E+02±56	99±41	5.9E+02±1.8E+02
	16384	11±3.7	34±1.3	6.9E+02±52	65±19	9.4E+02±3E+02
	32768	12±4.3	36±2.6	6.8E+02±36	87±28	5.1E+02±2E+02
0.01	4096	20±6.8	37±1.6	8.5E+02±1E+02	85±24	7.9E+02±4.1E+02
	8192	12±4.9	34±1.7	1.3E+03±7E+02	82±24	4E+02±1.5E+02
	16384	7.1±2.2	33±0.81	5.5E+02±47	1.1E+02±26	3.7E+02±68
	32768	10±4	31±0.97	4.8E+02±51	42±9.1	2.8E+02±98
0.1	4096	5.8±1.3	27±1.3	3.2E+02±32	8.1±1.7	33±9.2
	8192	5.9±1.3	26±1.3	3.1E+02±33	5.7±1	27±6.9
	16384	5.9±1.4	25±1	3.1E+02±34	4±1.4	26±7.7
	32768	5.1±1.1	25±1	3.1E+02±34	3.8±0.88	16±5.1
1	4096	14±5.3	29±1.3	4.3E+02±31	6.2±1.7	69±25
	8192	15±5.3	30±2.1	3.4E+02±38	5.6±2.2	69±25
	16384	16±5.6	28±1.1	4.1E+02±36	6.1±2	76±27
	32768	15±5.5	29±1.9	4.3E+02±38	5.6±1.5	73±24

epsilon	#target	rf1 (8)	rf2 (8)	wq (14)	oes10 (16)	oes97 (16)	scm1d (16)	scm20d (16)
0.001	4096	2E+13±2E+13	2E+13±2E+13	7.1E+09±3E+09	2.9E+08±8.3E+07	8.7E+08±4E+08	4E+07±3.6E+07	1.7E+07±1.1E+07
	8192	2E+13±2E+13	2E+13±2E+13	3.7E+09±1.9E+09	3.7E+08±1.3E+08	1.4E+09±1.2E+09	9.3E+05±5E+05	2.5E+08±1.9E+08
	16384	2E+13±2E+13	2E+13±2E+13	6.6E+09±3.2E+09	5.6E+08±4.3E+08	2.5E+08±1.3E+08	3.5E+05±1.3E+05	8.9E+07±5.7E+07
	32768	2E+13±2E+13	2E+13±2E+13	3.1E+09±1.2E+09	5.5E+08±3E+08	3.1E+08±9.5E+07	9.7E+05±4.5E+05	1.3E+09±1.3E+09
0.01	4096	2E+13±2E+13	2E+13±2E+13	1.1E+10±7.3E+09	4.3E+09±3.8E+09	3.5E+09±2.5E+09	4.1E+08±3.8E+08	1.3E+11±1.1E+11
	8192	2E+13±2E+13	2E+13±2E+13	6.4E+10±6E+10	3E+10±2.8E+10	1E+10±6.1E+09	8.1E+08±5.5E+08	1.1E+11±1.1E+11
	16384	2E+13±2E+13	2E+13±2E+13	3.3E+09±7.9E+08	1.1E+09±4.3E+08	1E+10±5.7E+09	4.8E+07±3.7E+07	1.3E+09±8.3E+08
	32768	2E+13±2E+13	2E+13±2E+13	5.1E+11±4.9E+11	6.5E+09±5E+09	4E+09±3.2E+09	1.6E+07±9.5E+06	2.7E+08±1.3E+08
0.1	4096	2E+13±2E+13	2E+13±2E+13	8.7E+09±3.7E+09	4.8E+04±3.2E+04	6E+09±6E+09	1.5E+03±6.7E+02	1.3E+06±6.4E+05
	8192	2E+13±2E+13	2E+13±2E+13	4.8E+09±1.5E+09	1.7E+05±1.3E+05	6E+09±6E+09	6.2E+02±2.8E+02	1.2E+06±8.7E+05
	16384	2E+13±2E+13	2E+13±2E+13	1.3E+10±6.8E+09	5.2E+04±4.7E+04	5.6E+09±5.6E+09	2.2E+02±46	2.9E+05±1E+05
	32768	2E+13±2E+13	2E+13±2E+13	7.4E+09±2.9E+09	7.6E+03±5.1E+03	9.2E+07±8.1E+07	1.1E+02±17	1.1E+05±3.1E+04
1	4096	2E+13±2E+13	2E+13±2E+13	8E+08±2E+08	6.6E+02±3.4E+02	8.3E+05±8.1E+05	4.1E+02±76	5.2E+05±6.5E+04
	8192	2E+13±2E+13	2E+13±2E+13	6.9E+08±1.7E+08	3.5E+02±1.8E+02	7.7E+05±7.6E+05	8.5E+02±3.1E+02	1.1E+06±3.9E+05
	16384	2E+13±2E+13	2E+13±2E+13	5.3E+08±1.2E+08	2.2E+02±1.5E+02	4E+05±4E+05	1.3E+02±14	4.7E+05±1.8E+05
	32768	2E+13±2E+13	2E+13±2E+13	5.5E+08±1.5E+08	1.9E+02±1.6E+02	3.1E+05±3.1E+05	1E+02±11	3.4E+05±6.4E+04

Table 1. Mean region size for varying ϵ and the number of target points in the ball.